University **POLITEHNICA** of Bucharest
Doctoral School of **AUTOMATIC CONTROL** and
COMPUTERS
SYSTEMS ENGINEERING

Ph.D. Thesis

ABSTRACT

Contribuții la optimizarea regimului de combustie al motoarelor Diesel

Contributions to the optimization of the combustion regime of Diesel engines

Ph.D. Student: **Eng. Mihaela-Ancuța Mone**

Ph.D. Coordinator: **Prof.dr.eng. Dumitru Popescu**

Bucharest
2021

Doctoral Commission:

President	Conf. dr. eng. Mihnea MOISESCU	from	„Politehnica" University of Bucharest
Scientific Coordinator	Prof. dr. eng. Dumitru POPESCU	from	„Politehnica" University of Bucharest
Member, Scientific Coordinator	Prof., Research Director Sette DIOP	from	CentraleSupelec, Université Paris-Saclay
Member	Prof. dr. eng. Radu-Emil PRECUP	from	„Politehnica" University of Timișoara
Member	Prof. dr. ing. Mircea IVĂNESCU	from	University of Craiova

Scientific Publications:

1. *Stochastic optimization and minimal risk problems*, Mihaela-Ancuța Mone, Sette Diop, Dumitru Popescu, 2017 14th International Workshop on Advanced Control and Diagnosis, Proceedings IFAC ACD 2017.
2. *Digital Control Ecosystem for Steel Plant Installations*, Dumitru Popescu, Ancuta Mone, Severus Constantin Olteanu, Lavinius Gliga, 2018 Academic Days of the Academy of Technical Sciences of Romania (ZASTR), ISSN 2066-6586.
3. *Optimal control of the combustion regime of an experimental Diesel Engine*, Mihaela-Ancuța Mone, Sette Diop, Dumitru Popescu, National Scientific Conference of the Academy of Romanian Scientist, vol. XIII, issue 1, 2019, ISSN 2601-5102.
4. *Optimal control for Diesel engine combustion regime*, Mihaela-Ancuța Mone, Sette Diop, Dumitru Popescu, 2019 22nd International Conference on Control Systems and Computer Science (CSCS), p. 42-47, DOI: 10.1109/CSCS47589.2019.
5. *Multi Model Control - MMC approach for nonlinear combustion regime of Diesel Engines*, 15th European Workshop on Advanced Control and Diagnosis(ACD 2019), Proceedings of the Workshop held in Bologna, Italy, on November 21–22, 2019, ISBN 978-3-030-85317-4, DOI 10.1007/978-3-030-85318-1, 2022.

6. *Optimal multi-model control for nonlinear systems with parametric uncertainties - Diesel Engine case study*, Mihaela-Ancuța Mone, Sette Diop, Dumitru Popescu, 2020 24th International Conference on System Theory, Control and Computing (ICSTCC), IEEE Catalog Number: CFP2036P-ART, ISBN: 978-1-7281-9809-5.
7. *Advanced Control for Hydrogen Pyrolysis Installations*, Dumitru Popescu, Catalin Dimon, Pierre Borne, Severus C. Olteanu, and Mihaela A. Mone, 2020, Energies 13, no. 12: 3270, https://doi.org/10.3390/en13123270.
8. *Evaluating the maximum domain of parameter model uncertainties in the combustion of a Diesel engine*, Mihaela-Ancuța Mone, Sette Diop, Dumitru Popescu, 2021 25th International Conference on System Theory, Control and Computing (ICSTCC), to be published in IEEE Xplore Digital Library.

Key-Words:

Automotive; Diesel engines; Emissions reduction; Mathematical modelling; Parametric uncertainties; Robust RST control; Robust LQR control; Multi-model multi-controller (MMMC control); Simulation; MATLAB/Simulink.

Contents

1. Introduction

The thesis represents a research in the automotive area, revealing the various technologies used for improving the environment and the passenger comfort, the strategies implemented by different constructors in Europe (e.g. Toyota Motor Corporation, Stellantis – comprised of PSA and FCA, Renault-Nissan-Mitsubishi Alliance, Hyundai Motor, Volkswagen AG, BMW Group, Ford, Daimler AG, Honda Motor, Volvo Cars, Jaguar Land Rover LTD, Mazda Motor Corporation) in order to respect the CAFÉ regulation which limits the CO_2 emissions to imposed thresholds, the negative impact the COVID-19 crisis had and continues to have on the automotive industry, and the tendencies on mobility which drive the development of electric mobility (i.e. HCCI and CAI engines, HEVC/EV/PHEV) [1-19].

The efforts and the efficacity of the measures undertaken to reduce the CO_2 emissions will be to no avail if the electric and hydrogen cars use electricity which is not produced by low-emissions systems. Therefore, the objective of the thesis consists of optimizing the combustion process of an experimental bench equipped with a Diesel engine, an Exhaust Gas Recirculation system (EGR) and a Variable Geometry Turbocharger (VGT) by controlling the intake manifold absolute pressure MAP and the mass air flow MAF produced by the VGT to the intake manifold. The bench is based in Amiens, France, at the University Picardie Jules Vernes.

Between September and December 2018 I did an traineeship at the Laboratoire des Signaux et Systèmes, at Centrale Supélec, University Paris-Saclay, where I benefited from the support of professor Sette Diop, co-director of this thesis, and researcher at CNRS (Fr. *Centre National de la Recherche Scientifique*).

Between September 2019 and January 2021, I participated in the A-Success project, *Dezvoltarea competențelor de antreprenoriat ale doctoranzilor și postdoctoranzilor – cheie a succesului în carieră*, MySMIS ID: 125125, where I obtained the first prize following the development of a business plan inspired by the Ph.D. thesis.

2. Mathematical modelling for the Diesel engine combustion process

The mathematical model of the engine is obtained working on the general gas equation [20]:

$$pV = \frac{m}{M}RT = \nu RT \tag{2.1}$$

where m is the amount of substance present in a tube of volume V, pressure p and the temperature T. M is the molecular mass of the gas and R is the ideal gas constant.

2.1. State-space linear invariant model

Reference [22] proposes an invariant state-space model associated to the Diesel engine, starting from the ideal gas equation, writing a differential equation for both the admission and evacuation cycle of the Diesel engine, and considering the dynamics of the power transfer of the compressor delayed by δ:

$$\begin{aligned} \dot{p}_i &= \frac{RT_i}{V_i}(F_i + F_{EGR} - F_{ie}) + \frac{\dot{T}_i}{T_i}p_i \\ \dot{p}_e &= \frac{RT_e}{V_e}\left(F_{ie} + F_f - F_{EGR} - F_{VGT}\right) + \frac{\dot{T}_e}{T_e}p_e \\ \dot{P}_C &= \frac{P_T - P_C}{\delta} \end{aligned} \tag{2.2}$$

The index *i* denotes the parameters at intake, *e* denotes the parameters at exhaust, p is the pressure, T is the temperature, V is the volume, R is the Reynolds constant, F_{EGR} is the flow through the EGR, F_{VGT} is

the flow through the VGT, F_{ie} – the flow through the intake manifold, F_f – the fuel flow, P_C – the compressor's power, P_T – the turbine's power.

By remodelling F_{EGR} and F_{VGT} as the equation of flow through a restriction, and considering the conservation of mass in an open system, (2.2) can be rewritten as a state-space representation [21]:

$$\begin{cases} \begin{pmatrix} \dot{p}_i \\ \dot{p}_e \\ \dot{P}_c \end{pmatrix} = A \begin{pmatrix} p_i \\ p_e \\ P_c \end{pmatrix} + B \begin{pmatrix} S_R \\ x_{VGT} \\ N \\ F_f \end{pmatrix} \\ \begin{pmatrix} F_i \\ p_i \end{pmatrix} = C \begin{pmatrix} p_i \\ p_e \\ P_c \end{pmatrix} + D \begin{pmatrix} S_R \\ x_{VGT} \\ N \\ F_f \end{pmatrix} \end{cases} \tag{2.3}$$

where the elements of the input vector are S_R - the surface of the EGR valve, x_{VGT} – the position of the VGT valve, N – the engine speed; the elements of the output vector are F_i – the mass air flow to be controlled and p_i – the manifold absolute pressure to be controlled.

2.2. State-space linear invariant reduced model

The inputs S_R and x_{VGT} are redefined based on the center of the actuator range, the fuel flow and the engine speed are considered constant and the following reduced invariant model is obtained [22]:

$$\begin{cases} \begin{pmatrix} \dot{p}_i \\ \dot{p}_e \\ \dot{P}_c \end{pmatrix} = A \begin{pmatrix} p_i \\ p_e \\ P_c \end{pmatrix} + B \begin{pmatrix} S_R \\ x_{VGT} \end{pmatrix} \\ \begin{pmatrix} F_i \\ p_i \end{pmatrix} = \begin{pmatrix} 0 & 0 & \dfrac{\eta_{CTT}}{c_p T_{amb}} \dfrac{1}{\left(\dfrac{p_i}{p_{amb}}\right)^{\gamma} - 1} \\ 1 & 0 & 0 \end{pmatrix} \begin{pmatrix} p_i \\ p_e \\ P_c \end{pmatrix} \end{cases} \tag{2.4}$$

2.3. Stability, controllability and observability analysis

The system is stable if the system matrix, $\boldsymbol{A}$, from (2.3) and (2.4) has all the eigenvalues in the left half plane.

A system whose state-space representation is given by (2.3) or (2.4), is controllable if the rank of the controllability matrix [23]:

$$M_C = [B \quad AB \quad A^2B \quad \cdots \quad A^{n-1}B] \tag{2.5}$$

is the same as the rank of $\boldsymbol{A}$, meaning there is a command acting on the output of the system.

A system whose state-space representation is given by (2.3) or (2.4), is observable if the rank of the observability matrix [23]:

$$M_O = \begin{bmatrix} C \\ CA \\ CA^2 \\ \vdots \\ CA^{n-1} \end{bmatrix} \tag{2.6}$$

is the same as the rank of $\boldsymbol{A}$, meaning the dynamic system is able to determine the state by working on the measured output $y = \begin{pmatrix} F_i \\ p_i \end{pmatrix}$.

2.4. Experimental results

2.4.1. Invariant model

For the simulation of the invariant model with 4 inputs and 2 outputs from (2.3), we consider the following numerical values for the matrices A, B and C:

$$A = \begin{bmatrix} -3{,}625 & 0 & 373{,}0841 \\ 35{,}3698 & -93{,}4776 & 0 \\ 0 & 0{,}026 & -9{,}0909 \end{bmatrix}$$

$$B = 10^5 + 0{,}05 \begin{bmatrix} 0{,}5714 & 0 & -0{,}000003 & 0 \\ -5{,}5755 & 0{,}1020 & 0{,}00003 & 1{,}4608 \\ 0 & -0{,}0002 & 0 & 0 \end{bmatrix} \quad (2.7)$$

$$C = \begin{bmatrix} 0 & 0 & 0{,}0249 \\ 1 & 0 & 0 \end{bmatrix}$$

$$D = \begin{bmatrix} 0 & 0 & 0 & 0 \\ 0 & 0 & 0 & 0 \end{bmatrix}$$

We compute the controllability matrix using (2.5). The rank of the controllability matrix is 3, equal to the rank of the matrix A from (2.7), therefore the invariant system is controllable.

We compute the observability matrix using (2.6). The rank of the observability matrix is 3, equal to the rank of the matrix A from (2.7), therefore the invariant system is observable.

The dynamics of the invariant model (2.3) can be observed in figure 2.1.

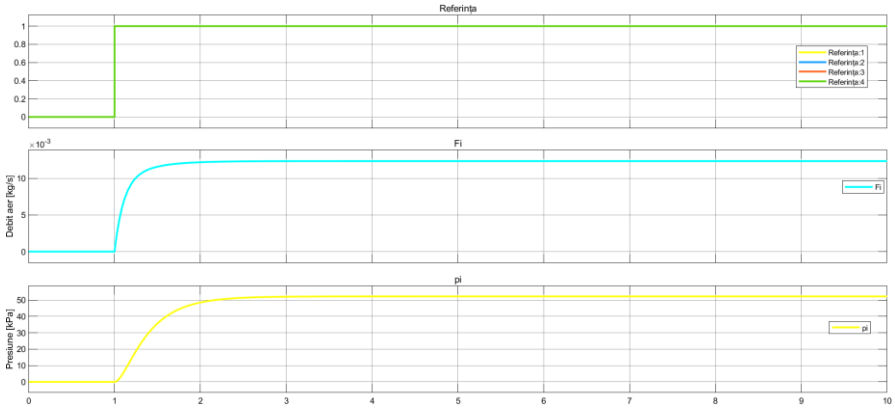

Fig. 2.1. Dynamics of the invariant model

The first signal in the above plot represents the set-point, the second is the mass air flow F_i (kg/s), and the third – the pressure p_i (kPa).

2.4.2. Reduced invariant model

For the simulation of the reduced invariant model with 2 inputs and 2 outputs from (2.4), we consider the following numerical values for the matrices A, B and C:

$$A_r = \begin{bmatrix} -3{,}625 & 0 & 373{,}0841 \\ 35{,}3698 & -93{,}4776 & 0 \\ 0 & 0{,}026 & -9{,}0909 \end{bmatrix}$$
$$B_r = \begin{bmatrix} 57140 & 0 \\ -557550 & 10200 \\ 0 & -20 \end{bmatrix} \qquad (2.8)$$
$$C_r = \begin{bmatrix} 0 & 0 & 0{,}0249 \\ 1 & 0 & 0 \end{bmatrix}$$
$$D_r = \begin{bmatrix} 0 & 0 \\ 0 & 0 \end{bmatrix}$$

We compute the controllability matrix using (2.5). The rank of the controllability matrix is 3, equal to the rank of the matrix A from (2.8), therefore the invariant system is controllable.

We compute the observability matrix using (2.6). The rank of the observability matrix is 3, equal to the rank of the matrix A from (2.8), therefore the invariant system is observable.

The dynamics of the reduced invariant model (2.4) can be observed in figure 2.2.

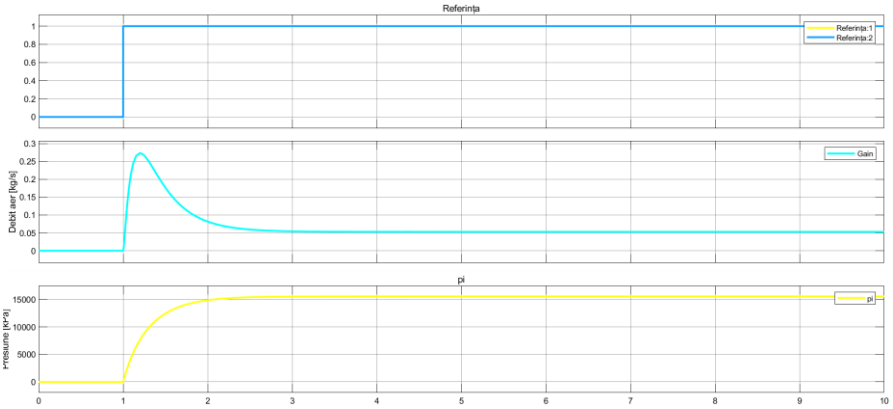

Fig. 2.2. Dynamics of the reduced invariant model

The first signal in the above plot represents the set-point, the second is the mass air flow F_i (kg/s), and the third – the pressure p_i (kPa).

Both the state-space invariant model and the reduced invariant model are stable, controllable and observable, therefore they can be used in the design phase of the control algorithms corresponding to the mass air flow F_i and the manifold absolute pressure p_i.

3. RST controller

3.1. General form of the RST command

The general form of the RST command is [21]:

$$u[k] = \begin{bmatrix} \frac{T(q^{-1})}{S(q^{-1})} & -\frac{R(q^{-1})}{S(q^{-1})} \end{bmatrix} \begin{bmatrix} r[k] \\ y[k] \end{bmatrix}, \forall k \in \mathbb{N}$$
$$R(q^{-1}) = r_0 + r_1 q^{-1} + \cdots + r_{n_r} q^{-n_r} \quad (3.1)$$
$$S(q^{-1}) = s_0 + s_1 q^{-1} + \cdots + s_{n_s} q^{-n_s}$$
$$T(q^{-1}) = t_0 + t_1 q^{-1} + \cdots + t_{n_t} q^{-n_t}$$

where $r[k]$ is the set-point, $u[k]$ – the command, $y[k]$ – the system's output, s_i, r_i, t_i – the parameters of the polynomial controller.

The schematic representation of the closed-loop system can be observed in figure 3.1.

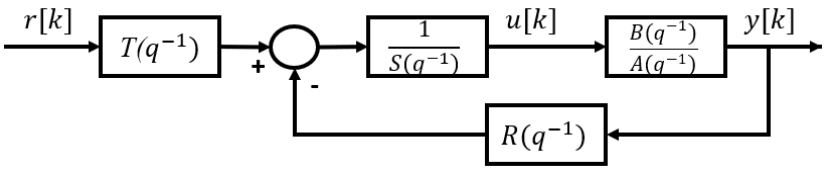

Fig. 3.1. RST closed-loop system

Based on the above figure, the closed-loop transfer function is:

$$H_{RST}(q^{-1}) = \frac{B(q^{-1})T(q^{-1})}{A(q^{-1})S(q^{-1}) + B(q^{-1})R(q^{-1})} \quad (3.2)$$

3.2. Pole-placement RST control

Through the pole placement strategy, the desired closed-loop poles contain the poles of the plant model:

$$P(q^{-1}) = 1 + p_1 q^{-1} + p_2 q^{-2} + \cdots + p_n q^{-n_p} = A(q^{-1})S(q^{-1}) + B(q^{-1})R(q^{-1}) \quad (3.3)$$

In order to solve the above polynomial equation, we start from the following matriceal form:

$$\boldsymbol{Mx} = \boldsymbol{p} \quad (3.4)$$

where:

$$\boldsymbol{x^T} = [1\ s_1\ s_2\ \dots\ s_{n_b+\delta}\ r_0\ r_1\ \dots\ r_{n_a-1}]$$
$$\boldsymbol{p^T} = [1\ p_1\ p_2\ \dots\ s_{n_a+n_b}] \quad (3.5)$$

$\boldsymbol{M}$ is the Sylvester matrix.

The coefficients of the polynomials $S(q^{-1})$ and $R(q^{-1})$ are obtained from the inverse of the matrix $\boldsymbol{M}$:

$$\boldsymbol{x} = \boldsymbol{M^{-1}p} \quad (3.6)$$

$T(q^{-1})$ is defined as follows:

$$T(q^{-1}) = GP(q^{-1}) = \begin{cases} \frac{1}{B(1)} P(q^{-1}), B(1) \neq 0 \\ P(q^{-1}), B(1) = 0 \end{cases} \quad (3.7)$$

3.3. Robust RST control

The robustness indicators taken into account in the thesis are: the modulus margin (ΔM) and the output sensitivity function ($S_{vy}(e^{-j\omega})$). They express the robustness of the control design in terms of the minimal distance with respect to the critical point (-1,0) in the Nyquist plane.

Figure 3.2. presents the modulus margin of an open-loop system.

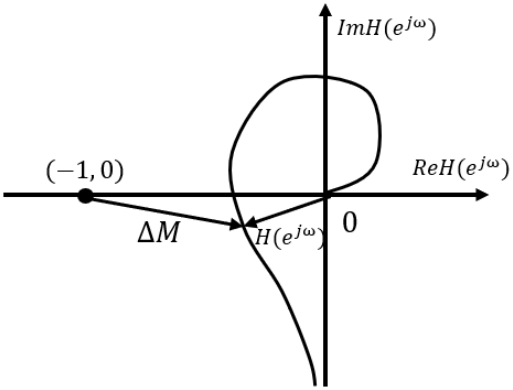

Fig. 3.2. Modulus margin ΔM

By definition:

$$\begin{aligned} \Delta M &= \min_{\omega\in\mathbb{R}}\left|1+H(e^{j\omega})\right| = \\ &= \min_{\omega\in\mathbb{R}}\sqrt{(1+re(H(e^{j\omega}))^2+im^2\left(H(e^{j\omega})\right)} \\ &= \min_{\omega\in\mathbb{R}}\frac{1}{\left|S_{vy}(e^{-j\omega})\right|} = \frac{1}{\max\limits_{\omega\in\mathbb{R}}\left|S_{vy}(e^{-j\omega})\right|} \end{aligned} \tag{3.8}$$

To obtain the modulus margin, it is therefore sufficient to simply plot the frequency characteristics of the modulus of the output sensitivity function in dB.

3.4. Experimental results – pole placement strategy

The direct input-output transfer functions for the two SISO systems are:

$$\begin{aligned} H_{EGR-p_i}(q^{-1}) &= \frac{280{,}8q^{-3}-102{,}9q^{-2}-273{,}6q^{-1}-99{,}2}{q^{-3}-2{,}271q^{-2}+1{,}617q^{-1}-0{,}3458} \\ H_{VGT-F_i}(q^{-1}) & \\ &= \frac{0{,}03711q^{-3}-0{,}0785q^{-2}+0{,}09375q^{-1}+0{,}02185}{q^{-3}-2{,}271q^{-2}+1{,}617q^{-1}-0{,}3458} \end{aligned} \tag{3.9}$$

The initial response for the $EGR - p_i$ and $VGT - F_i$ transfer are plotted in figures 3.3 and 3.4, respectively, for a time-step of $T_e =$ 0,01 s.

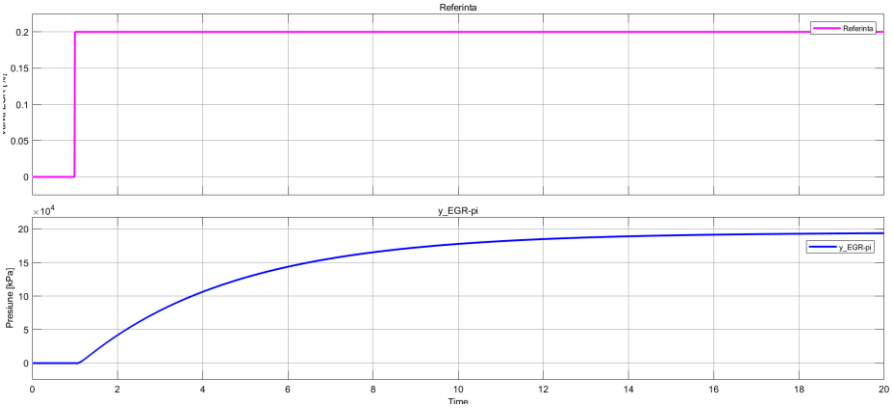

Fig. 3.3. Initial response of $EGR - p_i$ transfer

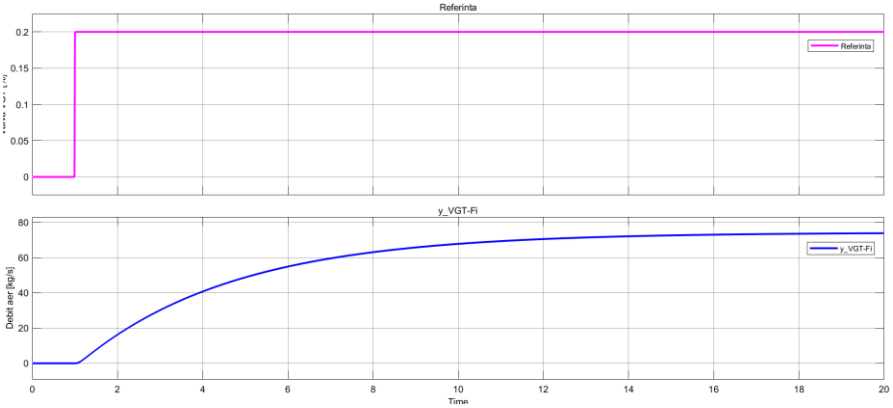

Fig. 3.4. Initial response of $VGT - F_i$ transfer

For the design of the RST controller through the pole placement strategy, we have chosen a second-order transfer function having the properties: natural pulsation, $\omega_n = 1\ \frac{rad}{s}$, and damping factor, $\zeta =$ 0,7.

For the EGR-p_i transfer:

$$R(q^{-1}) = \begin{bmatrix} -5{,}655 * 10^{-5} \\ -2{,}4735 * 10^{-4} \\ 3{,}0455 * 10^{-4} \end{bmatrix}$$

$$S(q^{-1}) = \begin{bmatrix} 0{,}9145 \\ 0{,}1916 \\ 0{,}0162 \end{bmatrix} \tag{3.10}$$

$$T(q^{-1}) = [-0{,}0051 \quad 0{,}0102 \quad -0{,}0051 \quad 0 \quad 0]$$

For the VGT-F_i transfer:

$$R(q^{-1}) = \begin{bmatrix} 0{,}4722 \\ 0{,}2139 \\ -0{,}6883 \end{bmatrix}$$

$$S(q^{-1}) = \begin{bmatrix} 1{,}0255 \\ 0{,}2810 \\ 0{,}0298 \end{bmatrix} \tag{3.11}$$

$$T(q^{-1}) = [13{,}4753 \quad -26{,}7619 \quad 13{,}2879 \quad 0 \quad 0]$$

The step-response of the closed-loop systems for the $EGR - p_i$ and $VGT - F_i$ transfer are plotted in figures 3.5 and 3.6, respectively.

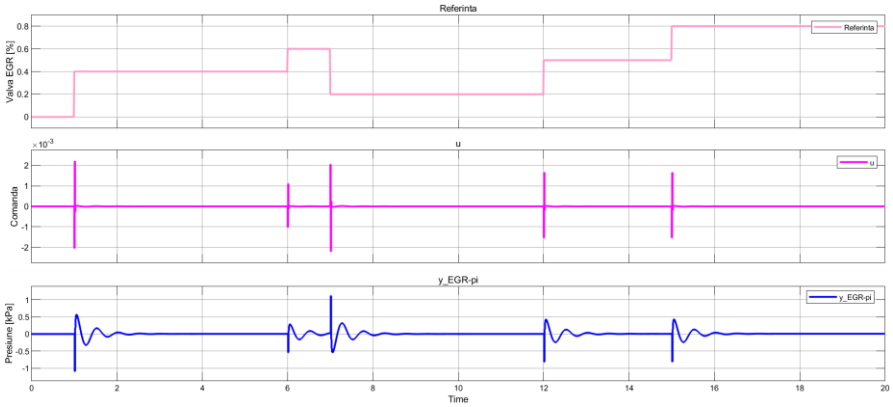

Fig. 3.5. $EGR - p_i$ closed-loop step-response

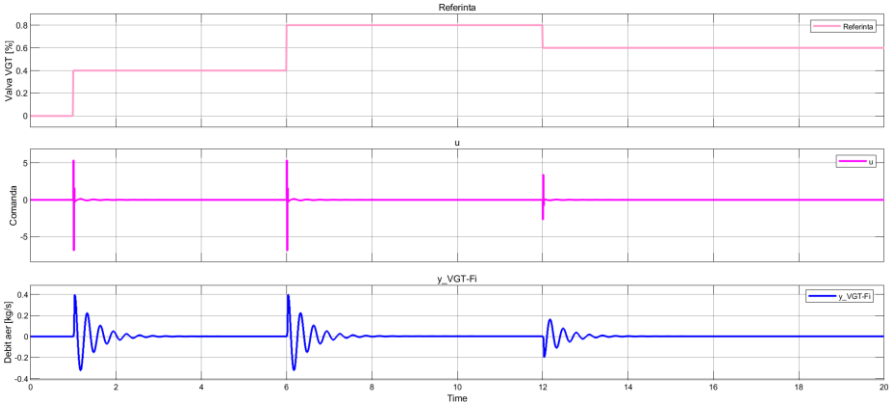

Fig. 3.6. $VGT - F_i$ closed-loop step-response

3.5. Experimental results – robust RST method

After applying the robust RST control alghorithm, we have obtained:

- EGR-p_i transfer:

$$R(q^{-1}) = \begin{bmatrix} 9{,}7915 * 10^{-4} \\ -0{,}0045 \\ 0{,}0062 \\ -0{,}0026 \end{bmatrix}$$

$$S(q^{-1}) = \begin{bmatrix} 1{,}7362 \\ 2{,}4217 \\ 1{,}346 \\ 0{,}2809 \end{bmatrix} \tag{3.12}$$

$$T(q^{-1}) = [-0{,}0026 \quad 0{,}0051 \quad -0{,}0025 \quad 0 \quad 0 \quad 0 \quad 0 \quad 0]$$

- VGT-F_i transfer:

$$R(q^{-1}) = \begin{bmatrix} -3{,}0995 \\ 14{,}4651 \\ -19{,}7220 \\ 8{,}3571 \end{bmatrix}$$

$$S(q^{-1}) = \begin{bmatrix} 0{,}6899 \\ 1{,}3483 \\ 1{,}2338 \\ 0{,}1958 \end{bmatrix} \tag{3.13}$$

$$T(q^{-1}) = [6{,}7376 \quad -13{,}3809 \quad 6{,}6440 \quad 0 \quad 0 \quad 0 \quad 0 \quad 0]$$

The step-response of the closed-loop systems for the $EGR - p_i$ and $VGT - F_i$ transfer are plotted in figures 3.7 and 3.8, respectively.

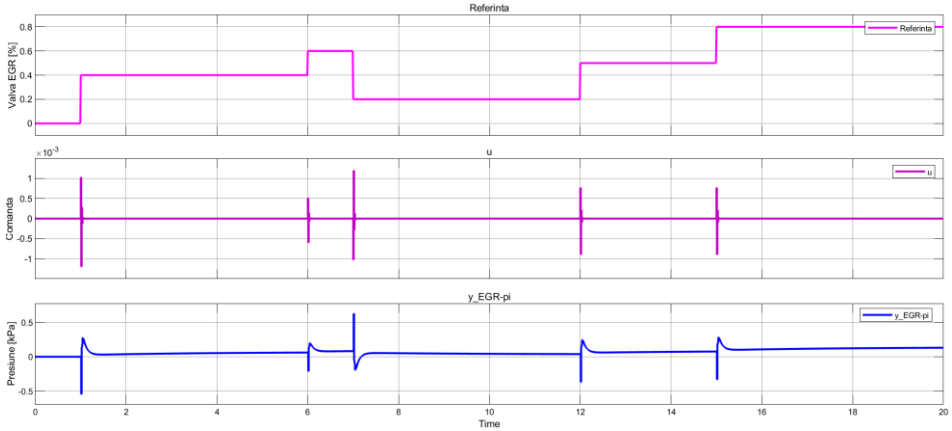

Fig. 3.7. p_i RST robust control

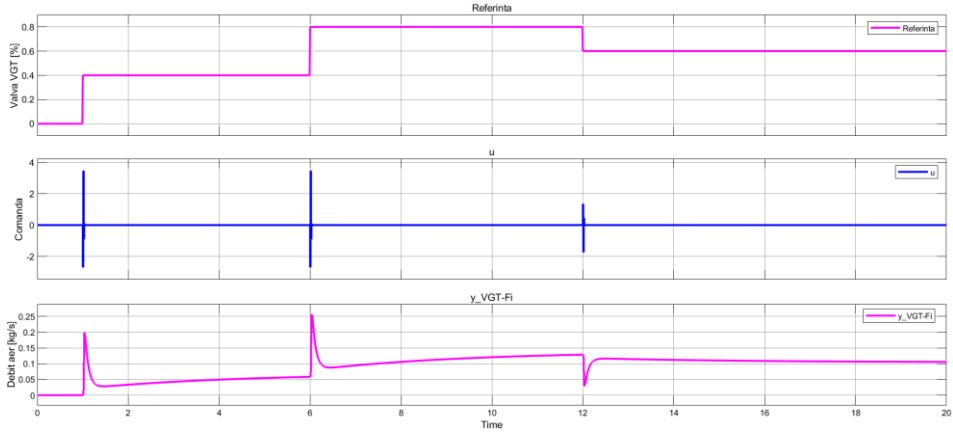

Fig. 3.8. F_i RST robust control

The results obtained in this chapter will be compared to the ones obtained in the next chapter where the system is presented in its state-space representation.

4. Evaluation of the maximum domain of parametric uncertainties for the combustion process

4.1. LQR control

LQR control consists in finding the command matrix $\boldsymbol{K}$ so that the command:

$$\begin{aligned} \boldsymbol{u}(t) &= -\boldsymbol{K}\boldsymbol{x}(t) \\ \boldsymbol{K} &= \boldsymbol{R}^{-1}\boldsymbol{B}^{T}\boldsymbol{P} \end{aligned} \tag{4.1}$$

can minimize the following performance index:

$$J(t) = \int_{0}^{\infty} \boldsymbol{x}^{T}(t)\boldsymbol{Q}\boldsymbol{x}(t) + \boldsymbol{u}^{T}(t)\boldsymbol{R}\boldsymbol{u}(t)dt \tag{4.2}$$

$\boldsymbol{P}$ from (4.1) is the solution of the Riccati equation:

$$\boldsymbol{A}^{T}\boldsymbol{P} + \boldsymbol{P}\boldsymbol{A} - \boldsymbol{P}\boldsymbol{B}\boldsymbol{R}^{-1}\boldsymbol{B}^{T}\boldsymbol{P} + \boldsymbol{Q} = 0 \tag{4.3}$$

The matrices $\boldsymbol{Q}$ and $\boldsymbol{R}$ can be chosen according to Bryson's rule [29]:

$$\begin{aligned} \boldsymbol{Q}_{ii} &= \frac{1}{maximum\ acceptable\ value\ of\ \boldsymbol{x}_i{}^2} \\ \boldsymbol{R}_{jj} &= \frac{1}{maximum\ acceptable\ value\ of\ \boldsymbol{u}_j{}^2} \end{aligned} \tag{4.4}$$

The function $V(\boldsymbol{x}) = \boldsymbol{x}^{T}\boldsymbol{P}\boldsymbol{x}$ is a Lyapunov function for the closed-loop system, and the following affirmations are true**:**

1. $V(\boldsymbol{x}) > 0, \boldsymbol{x} \neq 0$;
2. $\dot{V}(\boldsymbol{x}) = -\boldsymbol{x}^{T}(\boldsymbol{Q} + \boldsymbol{K}^{T}\boldsymbol{R}\boldsymbol{K})\boldsymbol{x} < 0, \boldsymbol{x} \neq 0$

(4.5)

4.2. Robust optimal control – parametric uncertainties

We consider the model of a linear time-invariant continuous system with the following state-space representation, where the modelling errors $\Delta\boldsymbol{A}$ and $\Delta\boldsymbol{B}$ affect the matrices $\boldsymbol{A}$ and $\boldsymbol{B}$, respectively:

$$\begin{cases} \dot{\boldsymbol{x}}(t) = (\boldsymbol{A} + \Delta\boldsymbol{A}(t))\boldsymbol{x}(t) + (\boldsymbol{B} + \Delta\boldsymbol{B}(t))\boldsymbol{u}(t) \\ \boldsymbol{y}(t) = \boldsymbol{C}\boldsymbol{x}(t) \end{cases} \tag{4.6}$$

The uncertainty domain is defined as follows:

$$D_i = \{(\Delta\boldsymbol{A}(t), \Delta\boldsymbol{B}(t) | \Delta\boldsymbol{A}^T\boldsymbol{A} \leq \alpha\boldsymbol{Q}_0, \Delta\boldsymbol{B} \leq \beta\boldsymbol{R}_0\} \tag{4.7}$$

where α, β are positive scalars, $\boldsymbol{Q}_0$ and $\boldsymbol{R}_0$ are symmetrical positive definite matrices.

The problem of interest is to find the maximum values of the scalars α, β so that the closed-loop system defined by (4.6) and (4.7) remains stable given the optimal command (4.1) [21].

The weight matrices $\boldsymbol{Q}_0$ and $\boldsymbol{R}_0$ are obtained from:

$$\begin{cases} Q = Q_0 + Q_1 \\ R = R_0 + R_1 \end{cases} \tag{4.8}$$

where $\boldsymbol{Q}$ and $\boldsymbol{R}$ are known from (4.2). $\boldsymbol{Q}_0$ and $\boldsymbol{R}_0$ are the matrices from (4.7); $\boldsymbol{Q}_1$ and $\boldsymbol{R}_1$ are symmetrical, positive definite matrices, and are obtained from (4.8).

If we consider $\boldsymbol{Q}$ and $\boldsymbol{R}$ as in (4.8) and we define the following symmetrical positive definite matrix:

$$\boldsymbol{\Psi} = \boldsymbol{P}^{-1}(\boldsymbol{Q}_1 + \boldsymbol{K}^T\boldsymbol{R}_1\boldsymbol{K})\boldsymbol{P}^{-1} \tag{4.9}$$

then the closed-loop system is stable for the uncertainties defined in the domain D_i (4.7) which satisfy:

$$\boldsymbol{\Psi} > (\alpha + \beta)\boldsymbol{I} \tag{4.10}$$

4.3. Experimental results

For the computation of the LQR command and the maximum domain of parametric uncertainties, 3 use cases were taken into account, for both the state-space linear invariant model, and the reduced invariant model.

4.3.1. State-space linear invariant model

1. Case 1:

$$\boldsymbol{Q} = \boldsymbol{C}^T\boldsymbol{C} = \begin{bmatrix} 1 & 0 & 0 \\ 0 & 0 & 0 \\ 0 & 0 & 0{,}006 \end{bmatrix}$$

$$\boldsymbol{R} = q^2\boldsymbol{I}_{4x4}, q \in \{1; 0{,}1; 0{,}01; 0{,}001\} \quad (4.11)$$

$$\boldsymbol{Q}_0 = \boldsymbol{B}\boldsymbol{B}^T = \begin{bmatrix} 4{,}058 & 3{,}82 & 4{,}0286 \\ 3{,}82 & 3{,}6818 & 3{,}7994 \\ 4{,}0286 & 3{,}7994 & 4 \end{bmatrix}$$

$\boldsymbol{R}_0 = \boldsymbol{I}_{4x4}$

We obtain $\boldsymbol{Q}_1 = \boldsymbol{Q} - \boldsymbol{Q}_0$ and $\boldsymbol{R}_1 = \boldsymbol{R} - \boldsymbol{R}_0$ from (4.8), and $\boldsymbol{\Psi}$ from (4.9).

Figure 4.1 presents the step-response of the closed-loop system for the 4 values of q, $q \in \{1; 0{,}1; 0{,}01; 0{,}001\}$.

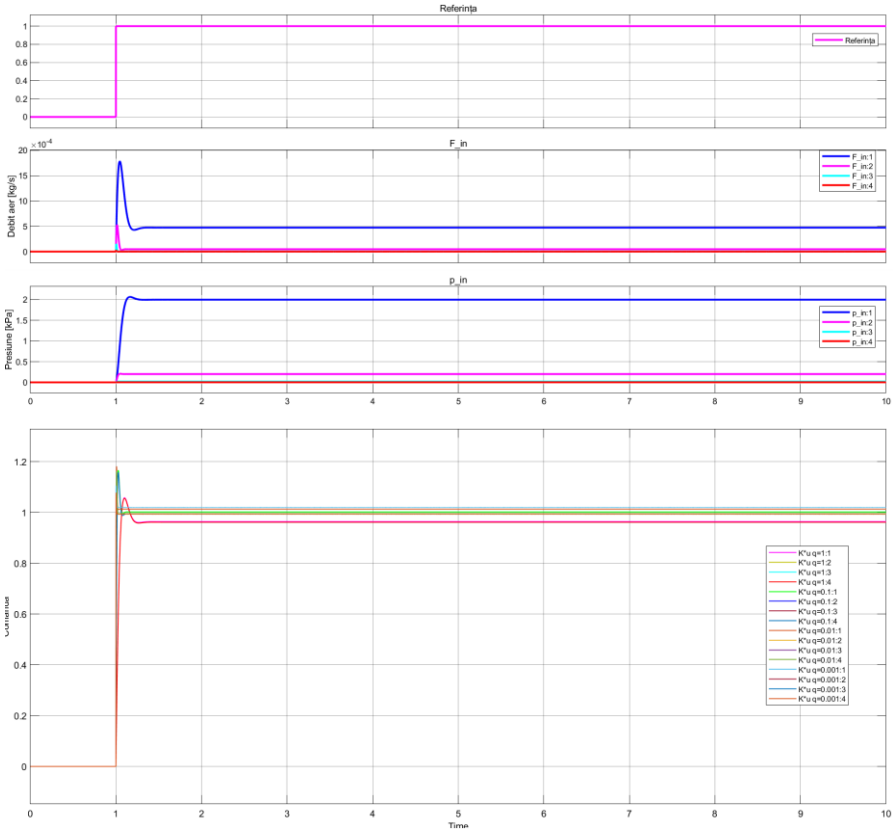

*Fig. 4.1. LQR comparison – **Q** is variable; **R** is constant*

2. Case 2:

$$\boldsymbol{Q} = \boldsymbol{C}^T\boldsymbol{C} = \begin{bmatrix} 1 & 0 & 0 \\ 0 & 0 & 0 \\ 0 & 0 & 6{,}2 * 10^{-4} \end{bmatrix}$$

$$\boldsymbol{R} = \boldsymbol{I}_{4x4} \tag{4.12}$$

$$\boldsymbol{Q}_0 = \boldsymbol{B}\boldsymbol{B}^T = \begin{bmatrix} 4{,}058 & 3{,}82 & 4{,}0286 \\ 3{,}82 & 3{,}6818 & 3{,}7994 \\ 4{,}0286 & 3{,}7994 & 4 \end{bmatrix}$$

$$\boldsymbol{R}_0 = q^2\boldsymbol{I}_{4x4}, q \in \{1; 0{,}1; 0{,}01; 0{,}001\}$$

Figure 4.2 presents the step-response of the closed-loop system for the 4 values of q, $q \in \{1; 0{,}1; 0{,}01; 0{,}001\}$.

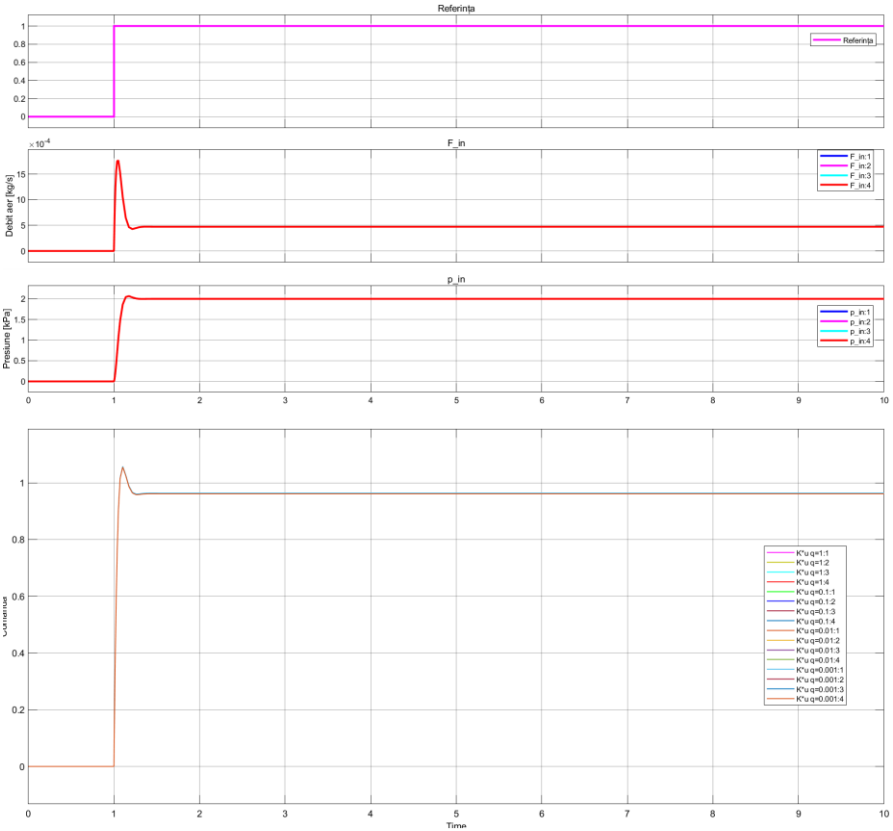

*Fig. 4.2. LQR comparison – **Q** is constant; **R** is varying*

3. Case 3:

Q and ***R*** are chosen according to Bryson's rule (4.4):

$$\boldsymbol{Q} = \begin{bmatrix} \frac{1}{\max(p_i)^2} & 0 & 0 \\ 0 & \frac{1}{\max(p_e)^2} & 0 \\ 0 & 0 & \frac{1}{\max(P_C)^2} \end{bmatrix} => \boldsymbol{Q}$$

$$= \begin{bmatrix} \frac{1}{165^2} & 0 & 0 \\ 0 & \frac{1}{200^2} & 0 \\ 0 & 0 & 1 \end{bmatrix}$$

$$\boldsymbol{R} = \begin{bmatrix} \frac{1}{\max(S_R)^2} & 0 & 0 & 0 \\ 0 & \frac{1}{\max(x_{VGT})^2} & 0 & 0 \\ 0 & 0 & \frac{1}{\max(N)^2} & 0 \\ 0 & 0 & 0 & \frac{1}{\max(F_f)^2} \end{bmatrix} \quad (4.13)$$

$$=> \boldsymbol{R} = \begin{bmatrix} \frac{1}{100^2} & 0 & 0 & 0 \\ 0 & \frac{1}{100^2} & 0 & 0 \\ 0 & 0 & \frac{1}{1800^2} & 0 \\ 0 & 0 & 0 & 1 \end{bmatrix}$$

$\boldsymbol{Q}_0 = \boldsymbol{B}\boldsymbol{B}^T$

$\boldsymbol{R}_0 = q^2\boldsymbol{I}_{4x4}, q \in \{1; 0{,}1; 0{,}01; 0{,}001\}$

Figure 4.3 presents the step-response of the closed-loop system for the 4 values of q, $q \in \{1; 0{,}1; 0{,}01; 0{,}001\}$.

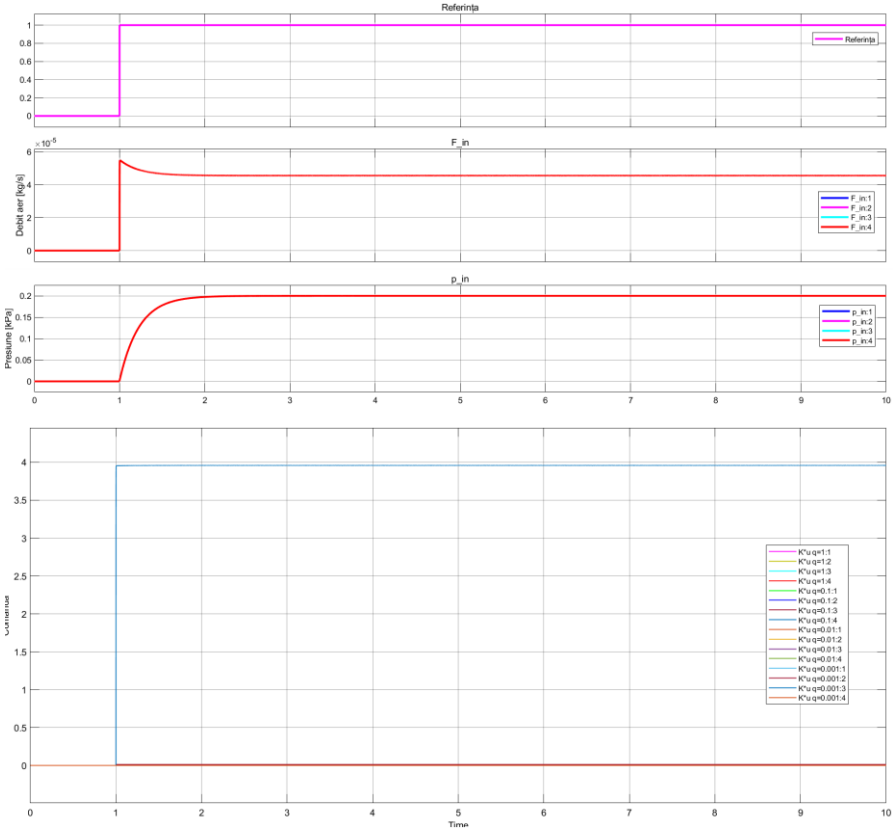

*Fig. 4.3. LQR comparison – **Q** is constant; **R** is varying*

4.3.2. State-space linear invariant reduced model

1. Case 1:

$$\boldsymbol{Q_r} = \boldsymbol{C_r}^T \boldsymbol{C_r} = \begin{bmatrix} 1 & 0 & 0 \\ 0 & 0 & 0 \\ 0 & 0 & 6{,}2001 * 10^{-4} \end{bmatrix}$$

$$\boldsymbol{R_r} = q^2 \boldsymbol{I}_{2x2}, q \in \{1; 0{,}1; 0{,}01; 0{,}001\} \tag{4.14}$$

$$\boldsymbol{Q}_0 = \boldsymbol{B_r} \boldsymbol{B_r}^T$$

$$= \begin{bmatrix} 3{,}265 * 10^9 & -3{,}1858 * 10^{10} & 0 \\ -3{,}1858 * 10^{10} & 3{,}1097 * 10^{11} & -204000 \\ 0 & -204000 & 400 \end{bmatrix}$$

$\boldsymbol{R_0}$=$\boldsymbol{I_{2x2}}$

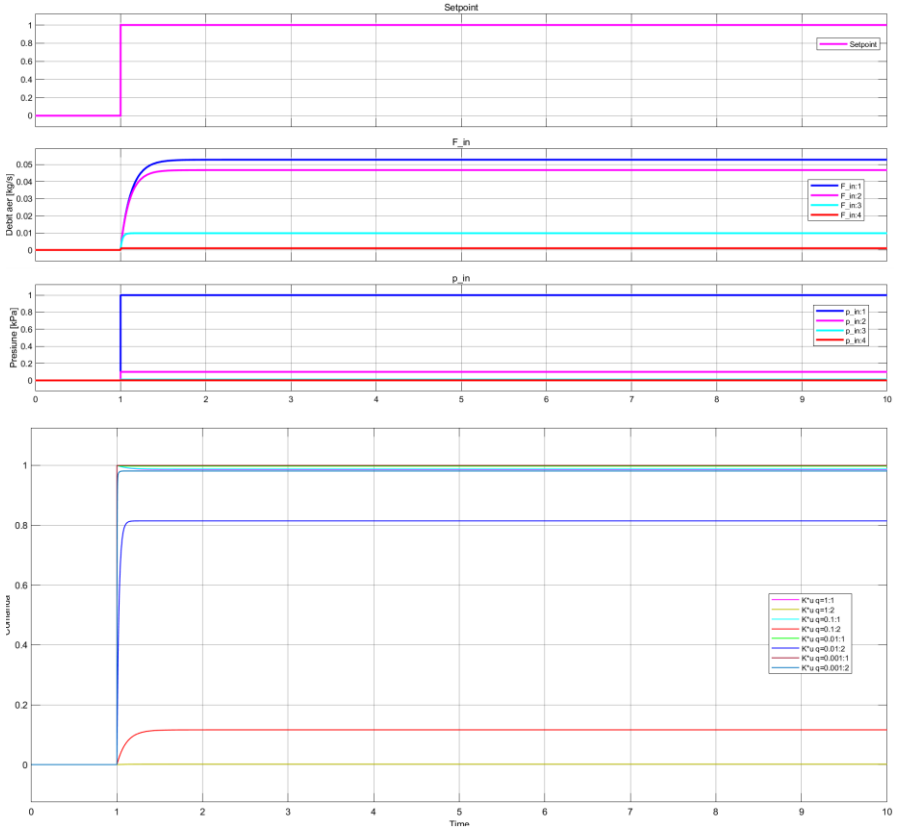

Fig. 4.4. LQR comparison – $\boldsymbol{Q}$ is varying; $\boldsymbol{R}$ is constant

2. Case 2:

$$\boldsymbol{Q_r} = \boldsymbol{C_r}^T \boldsymbol{C_r} = \begin{bmatrix} 1 & 0 & 0 \\ 0 & 0 & 0 \\ 0 & 0 & 6{,}2 * 10^{-4} \end{bmatrix}$$

$$\boldsymbol{R} = \boldsymbol{I_{2x2}} \qquad (4.15)$$

$$\boldsymbol{Q_0} = \boldsymbol{B_r}\boldsymbol{B_r}^T$$

$$= \begin{bmatrix} 3{,}2650 * 10^9 & -3{,}1858 * 10^{10} & 0 \\ -3{,}1858 * 10^{10} & 3{,}1097 * 10^{11} & -204000 \\ 0 & -204000 & 400 \end{bmatrix}$$

$$\boldsymbol{R}_0 = q^2\boldsymbol{I}_{2x2}, q \in \{1; 0{,}1; 0{,}01; 0{,}001\}$$

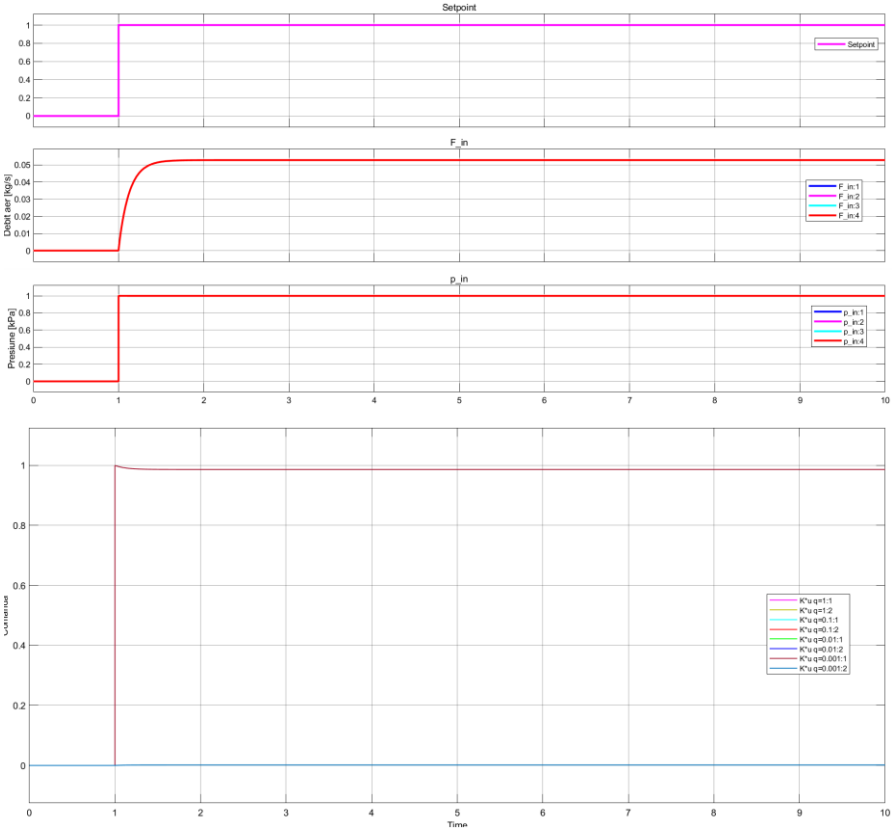

Fig. 4.5. LQR comparison – $\boldsymbol{Q}$ is constant; $\boldsymbol{R}$ is variable

3. Case 3:

$$\boldsymbol{Q_r} = \begin{bmatrix} \frac{1}{\max(p_i)^2} & 0 & 0 \\ 0 & \frac{1}{\max(p_e)^2} & 0 \\ 0 & 0 & \frac{1}{\max(P_C)^2} \end{bmatrix} => \boldsymbol{Q_r} = \tag{4.16}$$

$$\begin{bmatrix} \frac{1}{165^2} & 0 & 0 \\ 0 & \frac{1}{200^2} & 0 \\ 0 & 0 & 1 \end{bmatrix};$$

$$\boldsymbol{R_r} = \begin{bmatrix} \frac{1}{\max(S_R)^2} & 0 \\ 0 & \frac{1}{\max(x_{VGT})^2} \end{bmatrix} => \boldsymbol{R_r} = \begin{bmatrix} \frac{1}{100^2} & 0 \\ 0 & \frac{1}{100^2} \end{bmatrix}$$

$$\boldsymbol{Q_0} = \boldsymbol{B_r}\boldsymbol{B_r}^T$$

$$\boldsymbol{R_0} = q^2\boldsymbol{I_{2x2}}, q \in \{1; 0{,}1; 0{,}01; 0{,}001\}$$

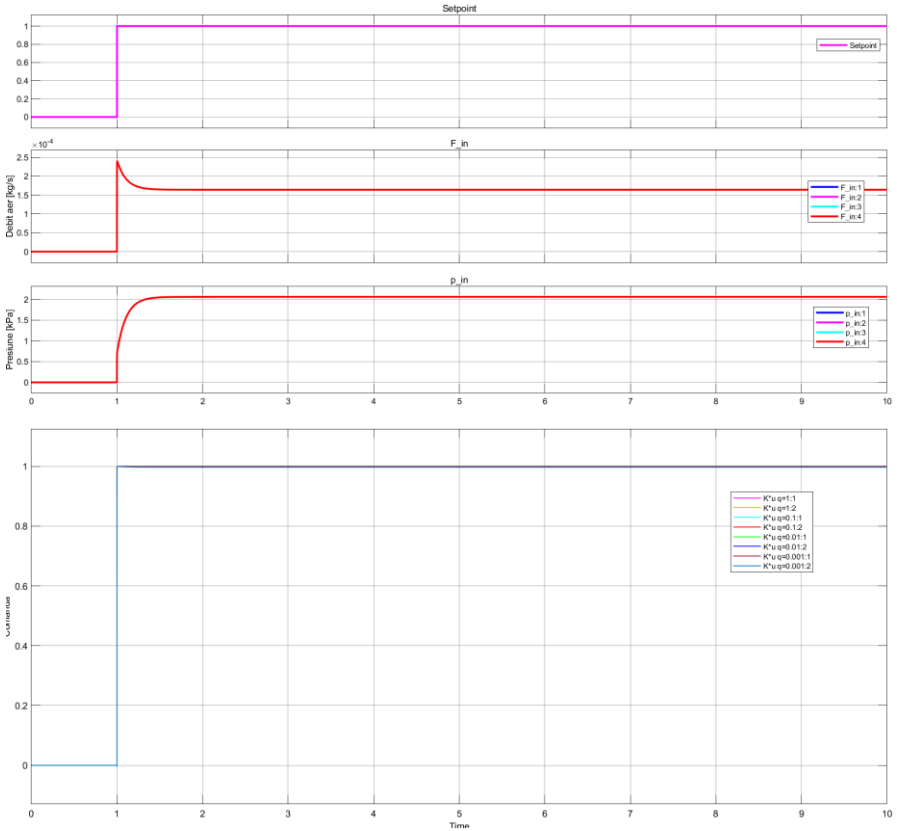

*Fig. 4.5. LQR comparison – **Q** is constant; **R** is variable*

Using the Control System Designer Toolbox from Simulink, as well as MATLAB scripts, we obtained the performance indicators for the RST and LQR control, which are listed in Table 4.1.

			Step Response from Setpoint r to Output y						
			Peak Amplitude	**Overshoot (%)**	**Rise Time (s)**	**Settling Time (s)**	**Steady State**	**Gain Margin CL (dB)**	**Modulus Margin OL (dB)**
RST		p_i	-2,74	73,9 la t=0,01 s	0,0128	39	1	5,07	40,99
		F_i	0,996	0 la t>100 s	0,0175	71,9	1	4,03	0,2991
RST Robust		p_i	1,37	394 la t=0,01s	0,000811	1,85	-0,175	7,57	40,99
		F_i	-0,495	251 la t=0,03 s	0,0103	3,53	-0,141	7,33	0,2991
LQR – model invariant	$q = 1$	p_i	0,518	3,44 la t=0,164 s	0,0803	0,209	0,501	-6,03	0,5885
		F_i	0,000447	276 la t=0,0455s	0,00413	0,257	0,000117	-64,2	1
	$q = 0{,}1$	p_i	0,0523	4,02 la t=0,0484s	0,0242	0,0651	0,0503	-26	0,5885
		F_i	0,000133	983 la t=0,0132s	0,0004128	0,0809	$1{,}05 * 10^{-3}$	-74,1	1
	$q = 0{,}01$	p_i	0,00521	2,88 la t=0,0138s	0,00656	0,0176	0,00507	-45,9	0,5885
		F_i	$3{,}88 * 10^{-5}$	2253 la t=0,00398s	0,000349	0,0173	$-1{,}94 * 10^{-6}$	-85	1
	$q = 0{,}001$	p_i	0,000513	0,554 la t=0,00345	0,00105	0,00174	0,00051	-65,9	0,5885
		F_i	$8{,}59 * 10^{-6}$	1348 la t=0,00107s	$2 * 10^{-5}$	0,0117	$5{,}93 * 10^{-7}$	-99,6	1
	Regula	p_i	0,0549	0 la t>1,8s	0,503	0,893	0,0484	-25,2	0,5885
		F_i	$1{,}37 * 10^{-5}$	19,85 la t=0,0043s	0,000716	0,53	$1{,}12 * 10^{-5}$	-97,2	1

LQR – model invariant redus	$q = 1$	$\boldsymbol{p_i}$	1	$2{,}76 * 10^{-6}$ la t=0,0004s	$3{,}96 * 10^{-5}$	$6{,}87 * 10^{-5}$	1	$-1{,}76 * 10^{-8}$	1
		$\boldsymbol{F_i}$	-0,0528	0 la t>0,9s	0,274	0,487	-0,0528	-25,5	0,9471
	$q = 0{,}1$	$\boldsymbol{p_i}$	0,1	$3{,}95 * 10^{-8}$ la t= $6{,}12 * 10^{-5}\ s$	$1{,}63 * 10^{-5}$	$1{,}99 * 10^{-5}$	0,1	-20	1
		$\boldsymbol{F_i}$	-0,0467	0 la t>0,8s	0,242	0,431	-0,0468	-26,6	0,9471
	$q = 0{,}01$	$\boldsymbol{p_i}$	0,01	$3{,}95 * 10^{-8}$ la t=$8{,}9 * 10^{-6}\ s$	$3{,}58 * 10^{-6}$	$4{,}39 * 10^{-6}$	0,01	-40	1
		$\boldsymbol{F_i}$	-0,0098	0 la t>0,14s	0,0498	0,0909	-0,00983	-40,2	0,9471
	$q = 0{,}001$	$\boldsymbol{p_i}$	-0,001	$5{,}49 * 10^{-9}$ la t= $1{,}83 * 10^{-5}$	$1{,}47 * 10^{-5}$	$1{,}82 * 10^{-5}$	-0,001	-60	1
		$\boldsymbol{F_i}$	-0,001	0 la t>0,06s	0,00446	0,00815	-0,001	-60	0,9471
	Regula Bryson	$\boldsymbol{p_i}$	1,57	0 la t>0,8s	0,228	0,398	1,58	3,95	1
		$\boldsymbol{F_i}$	-0,000237	0,0189 la t=0,00667	0,00105	0,00186	-0,000237	-72,5	0,9471

Table 4.1. RST control versus LQR control

5. Multi-model multi-controller design

The multi-model control structure for the three operating points can be observed in figure 5.1, where r is the set-point, (A_i, B_i, C_i, D_i) represent the minimal state-space realizations corresponding to the models for different operating points, $i \in \{1,2,3\}$. P represents the combustion process to be controlled, K_i represent the controllers, u_i represent the commands.

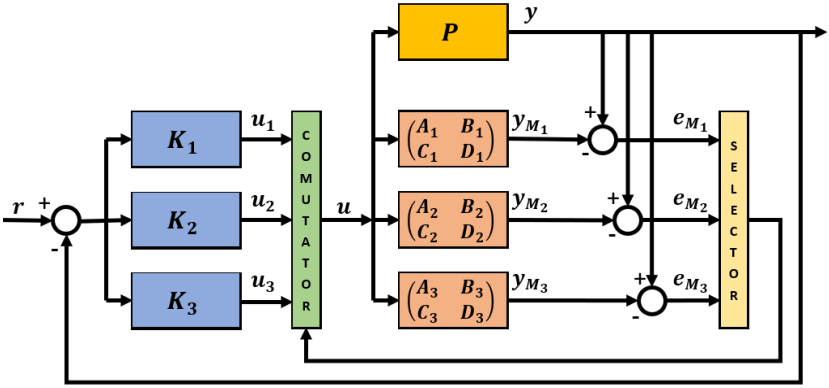

Fig. 5.1. Multi-model multi-controller (MMMC) structure

e_{M_i} is the modelling error, defined as the difference between the process' output, y, and the models' output, y_{M_i}. COMUTATOR (eng. *switch*) is the commutation law, based on the value of the following performance index:

$$\|e_{M_i}\| < epsilon \qquad (5.1)$$

where $epsilon$ is a threshold a-priori established.

Considering the state-space representation of the systems (2.3) and (2.4) and the vectorial form of the output, $y = \begin{bmatrix} F_i \\ p_i \end{bmatrix}$, we have:

$$\|e_{M_i}\| = \|y - y_{M_i}\| = \left\|\begin{bmatrix} F_i \\ p_i \end{bmatrix} - \begin{bmatrix} \hat{F}_i \\ \hat{p}_i \end{bmatrix}\right\| = \left\|\begin{bmatrix} F_i - \hat{F}_i \\ p_i - p_i \end{bmatrix}\right\| = \sqrt{\left(F_i - \hat{F}_i\right)^2 + (p_i - \hat{p}_i)^2} < epsilon \quad (5.2)$$

The controller K_i, which drives the process P, corresponds to the model M_i which offers the smallest modelling error, e_{M_i}. If, during simulation, the modelling error meets the condition of the criterion (5.2) for multiple models M_i simultaneously, then the algorithm will keep the value of command previously computed.

The main purpose of the robustness analysis of the LQR command designed in Chapter 4 (i.e. evaluating the maximum domain of parametric uncertainties) was to establish the minimal dimension of the MMMC configuration, therefore to have a minimum number of commutations and a reduction of computing effort in the design of the MMMC configuration.

5.1. Single-input single-output MMMC control

5.1.1. Input/Output MMMC representation

For the $EGR - p_i$ transfer, we have the following 3 models:

$$\begin{aligned} B_{1p_i} &= [280{,}8 \quad -102{,}9 \quad -273{,}6 \quad -99{,}22\ ] \\ B_{2p_i} &= [210 \quad -56{,}8 \quad -198{,}45 \quad -77{,}28] \\ B_{3p_i} &= \quad [178{,}5 \quad -12{,}7 \quad -102{,}33 \quad -24{,}44] \\ A_{p_i} &= [1 \quad -2{,}271 \quad 1{,}617 \quad -0{,}3458] \end{aligned} \quad (5.3)$$

For $VGT - F_i$ transfer, we have the following 3 models:

$$B_{1F_i} = [0{,}03711 \quad -0{,}0785 \quad 0{,}09375 \quad 0{,}02185] \quad (5.4)$$

$$B_{2F_i} = [0{,}02899 \quad -0{,}0622 \quad 0{,}08945 \quad 0{,}01765]$$

$$B_{3F_i} = \quad [0{,}02489 \quad -0{,}0558 \quad 0{,}08012 \quad 0{,}01247]$$

$$A_{F_i} = [1 \quad -2{,}271 \quad 1{,}617 \quad -0{,}3458]$$

After applying the robust RST control algorithm presented in Chapter 3, we have obtained the dynamics of the closed-loop system, for both the pressure p_i (figure 5.2), and the mass air flow, F_i (figure 5.3).

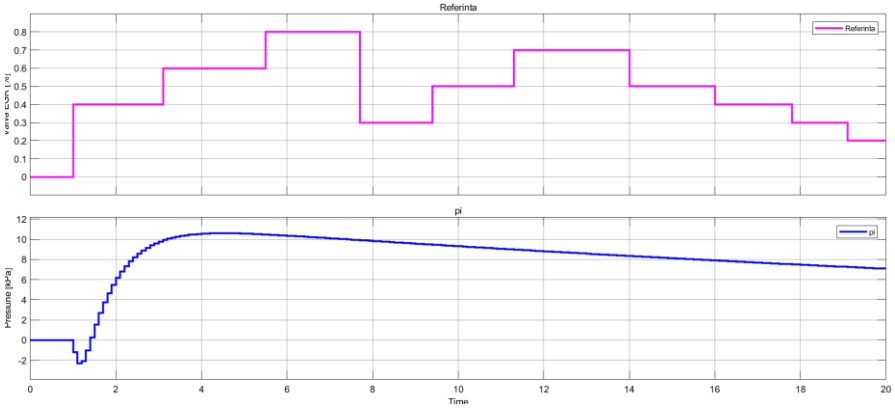

Fig. 5.2. RST MMMC SISO I/O p_i step response

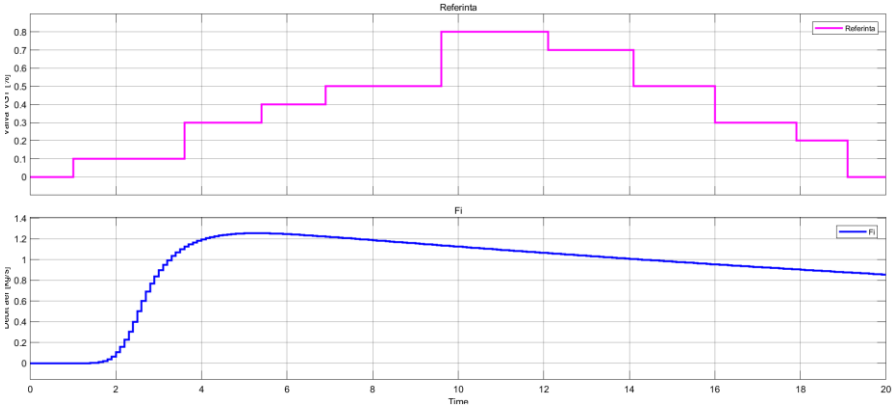

Fig. 5.3. RST MMMC SISO I/O F_i step response

5.1.2. State-space MMMC representation

For each model in (5.3) and (5.4) an equivalent state-space minimal realization was obtained. The process was represented by (3.9), and an equivalent minimal realization was computed. For each M_i model, an LQR controller, K_i, was designed, where $\boldsymbol{Q}$ and $\boldsymbol{R}$ are chosen as the identity matrices.

Figures 5.4 and 5.5 present the step response for the MMMC configuration for controlling p_i and F_i, respectively.

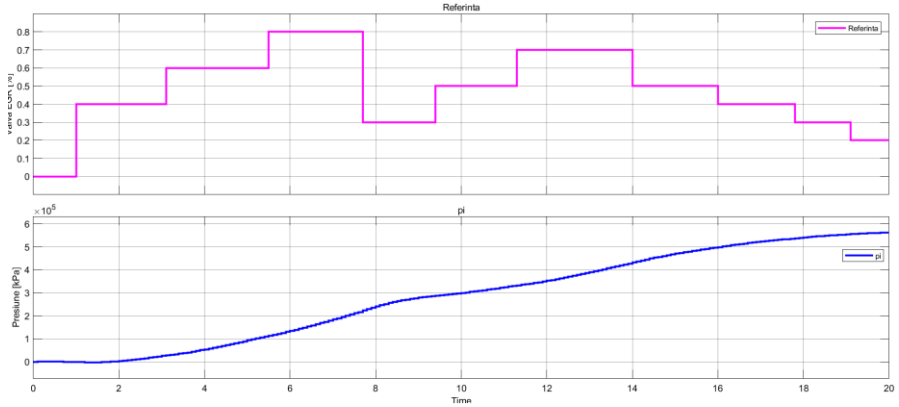

Fig. 5.4. LQR MMMC SISO SS p_i step response

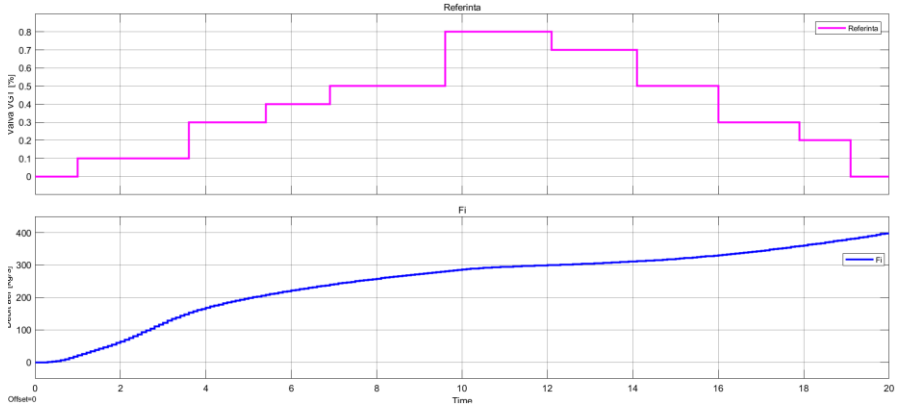

Fig. 5.5. LQR MMMC SISO SS F_i step response

5.2. Multiple-input multiple-output MMMC control

For the MIMO case, where the process is represented by (2.7) and (2.8), and the models M_i chosen based on the analysis in Chapter 4, the closed-loop system response is presented in figures 5.6 and 5.7, respectively.

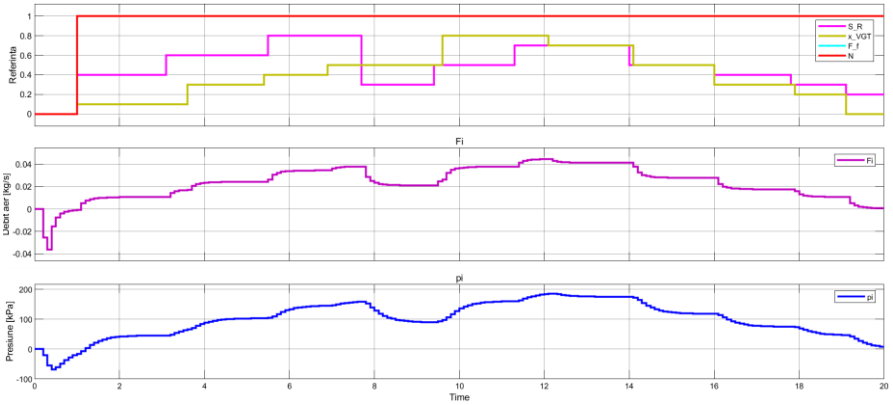

Fig. 5.6. MIMO LQR MMMC step response – invariant model

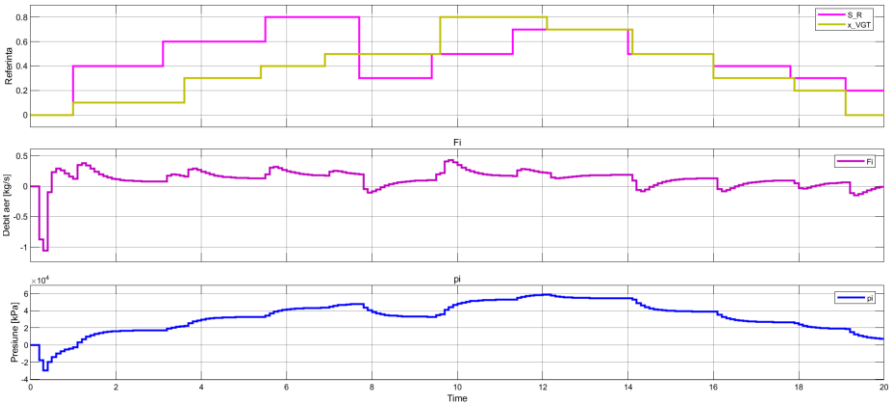

Fig. 5.7. MIMO LQR MMMC step response – reduced invariant model

The multi-model multi-controller approach brings consistent control improvements by selecting the adequate model based on the process' operating point and the corresponding controller.

6. Conclusions, personal contributions and future research

6.1. Conclusions

This automotive research reveals the various technologies used for improving the environment and the passenger comfort, the strategies implemented by different constructors in order to respect the CAFÉ regulation, the negative impact the COVID-19 crisis had and continues to have on the automotive industry, and the tendencies on mobility which drive the development of electric mobility.

The efficacity of the measures undertaken to reduce the CO_2 emissions will only take place if the electric and hydrogen cars use electricity produced by low-emissions systems. Until then, the optimization of the combustion regime of Diesel engines remains a subject of interest.

The non-linear mathematical models of the combustion regime of the Diesel engine were estimated. For the linearized and reduced mathematical models, both SISO and MIMO, state-space minimal realizations were obtained. Studies of stability, controllability and observability were conducted. These models were used in order to control the key parameters of the combustion process: manifold absolute pressure MAP and mass air flow MAF.

RST polynomial controllers were designed to control the direct transfer from the input EGR to p_i and VGT to F_i, respectively.

The evaluation of the maximum domain of parametric uncertainties for the LQR control was done as a pre-requisite for the multi-model multi-controller approach.

The RST and LQR controllers were used in designing the multi-model multi-controller (MMMC) structure. The novelty in the case of the MMMC approach consists in utilizing the MIMO system for the combustion process, whereas the comutation among models being done based on the minimum-norm model error.

The evaluation of the maximum domain of parametric uncertainties for the nonlinear combustion process played an important role in establishing the minimum points on the static characteristic so that we have a minimum number of commutations and a reduction of computing effort in the design of the MMMC configuration.

6.2. Personal contributions

State of the art analysis regarding the technologies used for improving the environment and the passenger comfort, the strategies implemented by different constructors in order to respect the CAFÉ regulation, the negative impact the COVID-19 crisis had and continues to have on the automotive industry, the tendencies on mobility which drive the development of electric mobility and the obstacles encountered in the era of electrification for a sustainable and safe transition.

Stability, controllability and observability analyses of the mathematical models of the combustion process, a pre-requisite for the design of the control algorithms.

Design of two control systems for the combustion process of the Diesel engine: LQR and RST, and a comparison of the performances of the two.

Evaluation of the maximum domain of parametric uncertainties and the robustness of the LQR control, as a pre-requisite for the design of the multi-model multi-controller structure.

Considering the MIMO system as the model for the combustion process in the MMMC configuration and the selection of the corresponding controller based on the value of the minimum-norm model error.

Development of the MATLAB scripts and the Simulink models in order to obtain the experimental results presented throughout the thesis.

6.3. Future research

1. Using Deep Learning to estimate the NO_x emissions [38], to assess the performance of on-board diagnosis. The challenge encountered by this approach consists in the large amount of computational effort required by those networks.
2. Using Reinforcement Learning [39] to control the manifold absolute pressure MAP and the mass air flow MAF. This technique has its roots in psychology and it implies training an agent by repeated experiences so that it makes the best choices based on the rewards it receives from the environment.
3. Solving the following optimization problem: maximization of the minimal eigenvalue of $\boldsymbol{\Psi}$ from (4.16) by means of non-

linear optimization techniques so that the matrices $\boldsymbol{Q}_1$ and $\boldsymbol{R}_1$ from (4.15) are optimal and the system is robust.

Bibliography

[1] *Fiches Techniques Environnement*, www.groupe.renault.com

[2] https://www.bosch-mobility-solutions.com/en/solutions/exhaust-gas-treatment/ denoxtronic- exhaust-gas-treatment-system/

[3] *En route vers la neutralité carbone*, Rapport Climat Avril 2021, Groupe Renault

[4] https://ec.europa.eu/clima/policies/transport/vehicles/regulation_en

[5] https://www.eea.europa.eu/data-and-maps/indicators/average-co2-emissions-from-motor-vehicles/assessment-2

[6] https://www.epa.gov/vw/learn-about-volkswagen-violations

[7] http://www2.paconsulting.com/rs/526-HZE-833/images/PA-CO2-Report-2019_2020.pdf

[8] *Strategia Groupe Renault pentru respectarea normei CAFE*: https://www.youtube.com/watch?v=NGzdji52d7E

[9] *Time-varying MPC-based energy management for HEV including engine stop & start*, Alexandra Stroe et al., 978-1-5090-2720-0, 2016.

[10] https://www.eea.europa.eu/data-and-maps/daviz/new-electric-vehicles-by-country-1#tab-chart_1

[11] https://pro.largus.fr/actualites/voitures-electriques-les-modeles-les-plus-vendus-en-europe-en-2020-10548393.html

[12] https://new.siemens.com/dk/da/virksomhedsoplysninger/innovation/pictures-of-the-future/futureofmobility.html

[13] https://www.bosch-mobility-solutions.com/en/mobility-topics/powertrain-and-electrified-mobility/synthetic-fuels/

[14] https://www.bosch-mobility-solutions.com/en/mobility-topics/powertrain-mix-for-better-air-quality/

[15] https://www.bosch-mobility-solutions.com/en/about-us/current-news/renewable-gasoline/

[16] https://www.bosch-mobility-solutions.com/en/mobility-topics/powertrain-and-electrified-mobility/gasoline-engine/

[17] https://www.bosch-mobility-solutions.com/en/mobility-topics/powertrain-and-electrified-mobility/

[18] https://www.adaptautomotive.com/articles/924-the-industrys-ev-obstacles

[19] https://www.acea.be/uploads/statistic_documents/Economic_and_Market_Report_full-year_2020.pdf

[20] *Internal Combustion Engine Fundamentals*, John B. Heywood, McGraw-Hill Education, 1st edition, 1988, ISBN: 0-07-028637-X.

[21] *Modelisation, identification et commande des systemes*, Genevieve Dauphin-Tanguy, Laurent Foulloy, Dumitru Popescu, Editura Academiei Române, 2004, ISBN: 973-27-1086-1.

[22] *Calibratable Linear Parameter-Varying Control of a Turbocharged Diesel Engine*, Merten Jung and Keith Glover, IEEE TRANSACTIONS ON CONTROL SYSTEMS TECHNOLOGY, VOL. 14, NO. 1, JANUARY 2006.

[23] *Teoria Sistemelor: culegere de probleme*, R. Ștefan, F. Stoican, S. Tudor, C. Oară, Editura Politehnica Press, București, 2013, ISBN: 978-606-515-517-6.

[24] *Optimal control of the combustion regime of an experimental Diesel engine*, Mihaela-Ancuța Mone, Sette Diop, Dumitru Popescu, National Scientific Conference of the Academy of Romanian Scientist, vol. XIII, issue 1, 2019, ISSN 2601-5102.

[25] *Multi-model adaptive control for turbocharged Diesel engines*, Silviu CÎRSTOIU, Dumitru POPESCU, U.P.B. Sci. Bull., Series C, Vol. 75, Iss. 1, 2013.

[26] *Advanced Control for Hydrogen Pyrolysis Installations*, Dumitru Popescu, Catalin Dimon, Pierre Borne, Severus Constantin Olteanu, Mihaela-Ancuța Mone, Energies 2020, 13, 3270; doi:10.3390/en13123270.

[27] *Digital control ecosystem for steel plant installations*, Dumitru POPESCU, Pierre BORNE, Mihaela-Ancuța MONE, Annals of the Academy of Romanian Scientists Series on Engineering Sciences, Volume 10, Number 1/2018, ISSN 2066-8570.

[28] *The R-S-T Digital Controller Design and Applications*, I. D. Landau, Control Engineering Practice 6(2):155-165, 1998.

[29] *Linear Systems Theory*, J. P. Hespanha,. Princeton, NJ, USA, Princeton University Press, 2009, ISBN: ISBN 978-0-691-14021-6.

[30] *Stochastic optimization and minimal risk problems*, Mihaela-Ancuța Mone, Sette Diop, Dumitru Popescu, 14th International Workshop on Advanced Control and Diagnosis (ACD), București, Romania, Proceedings IFAC ACD 2017.

[31] *Optimal control for Diesel engine combustion regime*, Mihaela-Ancuța Mone et al., 2019 22nd International Conference on Control Systems and Computer Science (CSCS), p. 42-47, DOI: 10.1109/CSCS47589.2019.

[32] *Evaluating the maximum domain of parameter model uncertainties in the combustion of a Diesel engine*, Mihaela-Ancuța Mone, Sette Diop, Dumitru Popescu, 25th International Conference on System Theory, Control and Computing (ICSTCC), Iași, Romania, 2021, to be published in IEEE Xplore Digital Library.

[33] *Multimodel Control of Diesel Engines*, Silviu Cirstoiu et al, 2017 J. Phys.: Conf. Ser. 783 012043.

[34] *Multiple-Model Design and Switching Solution for Nonlinear Processes Control*, C. Lupu, D. Popescu, C. Petrescu, Al. Ticlea, C. Dimon, A. Udrea, I. Bogdan, , ISC'08, The 6th Annual Industrial

Simulation Conference, Lyon, France, pp. 71-76, ISBN 978-90-77381-4-03, 2008.

[35] *A Simulator for the Multi-model Control of Diesel Engines*, Silviu CÎRSTOIU, Dumitru POPESCU, Studies in Informatics and Control, ISSN 1220-1766, vol. 23 (4), pp. 381-386, 2014.

[36] *Optimal Multi-Model Control for Nonlinear Systems with Parametric Uncertainties - Diesel Engine Case Study*, Mihaela-Ancuța Mone, Sette Diop, Dumitru Popescu, 2020 24th International Conference on System Theory, Control and Computing (ICSTCC), IEEE Catalog Number: CFP2036P-ART, ISBN: 978-1-7281-9809-5.

[37] *Multi Model Control - MMC approach for nonlinear combustion regime of Diesel Engines*, Mihaela-Ancuța Mone et al., 15th European Workshop on Advanced Control and Diagnosis (ACD 2019), Bologna, Italy, ISBN 978-3-030-85317-4.

[38]https://www.mathworks.com/company/newsletters/articles/using-deep-learning-networks-to-estimate-nox-emissions.html

[39] *Reinforcement Learning Toolbox User's Guide*, MATLAB R2021a, MathWorks